SCIENCE CHINA
Physics, Mechanics & Astronomy

• Article •

June 2017 Vol. 60 No. 6: 067711
doi: 10.1007/s11433-017-9020-8

Effects of $BaTiO_3$ and $SrTiO_3$ as the buffer layers of epitaxial $BiFeO_3$ thin films

Yu Feng[1,2], Can Wang[1,2*], ShiLu Tian[1,2], Yong Zhou[1,2], Chen Ge[1], HaiZhong Guo[1], Meng He[1], KuiJuan Jin[1,2,3*], and GuoZhen Yang[1,2,3]

[1] Beijing National Laboratory for Condensed Matter Physics, Institute of Physics, Chinese Academy of Sciences, Beijing 100190, China;
[2] University of Chinese Academy of Sciences, Beijing 100049, China;
[3] Collaborative Innovation Center of Quantum Matter, Beijing 100190, China

Received January 1, 2017; accepted March 3, 2017; published online April 19, 2017

$BiFeO_3$ (BFO) thin films with $BaTiO_3$ (BTO) or $SrTiO_3$ (STO) as buffer layer were epitaxially grown on $SrRuO_3$-covered $SrTiO_3$ substrates. X-ray diffraction measurements show that the BTO buffer causes tensile strain in the BFO films, whereas the STO buffer causes compressive strain. Different ferroelectric domain structures caused by these two strain statuses are revealed by piezoelectric force microscopy. Electrical and magnetical measurements show that the tensile-strained BFO/BTO samples have reduced leakage current and large ferroelectric polarization and magnetization, compared with compressively strained BFO/STO. These results demonstrate that the electrical and magnetical properties of BFO thin films can be artificially modified by using a buffer layer.

BFO, buffer layer, strain

PACS number(s): 68.60.Bs, 68.55.-a, 81.15.Aa, 84.37.+q

Citation: Y. Feng, C. Wang, S. L. Tian, Y. Zhou, C. Ge, H. Z. Guo, M. He, K. J. Jin, and G. Z. Yang, Effects of $BaTiO_3$ and $SrTiO_3$ as the buffer layers of epitaxial $BiFeO_3$ thin films, Sci. China-Phys. Mech. Astron. **60**, 067711 (2017), doi: 10.1007/s11433-017-9020-8

1 Introduction

As a promising candidate for many applications, such as spintronics, information storage and communication, multiferroic materials have attracted significant attention for their simultaneous ferroelectricity and (anti)ferromagnetism [1]. $BiFeO_3$ (BFO) is a remarkable multiferroic material due to its large spontaneous polarization, high Curie temperature (~820°C) and high Néel temperature (~370°C) [2]. BFO possesses a rhombohedrally distorted perovskite structure with space group *R3c* at room temperature [3]. A relative Bi-O displacement resulting from the stereochemical activity of the lone electron pair located on the Bi cation causes the ferroelectricity in bulk BFO [4,5]; its antiferromagnetism or weak ferromagnetism at room temperature is due to a residual moment from a canted spin structure [6,7].

BFO thin films have recently been intensively studied for their interesting physics and applications in nanoelectronic devices [8]. However, as do other ferroelectric materials, BFO thin films suffer from degradation in electrical properties owing to interfacial effects, space charge effects, residual stresses induced by lattice mismatch and thermal misfit, and defects such as oxygen vacancies [9-13]. The large leakage current in BFO thin films is one of the major issues that limit their application in electronic devices.

Some studies have shown that the physical properties of BFO thin films can be improved or modified by using an ap-

*Corresponding authors (Can Wang, email: canwang@iphy.ac.cn; KuiJuan Jin, email: kjjin@iphy.ac.cn)

© Science China Press and Springer-Verlag Berlin Heidelberg 2017

propriate buffer [14]. It has been demonstrated that introducing an insulating oxide layer with lower leakage current to form a double-layered or multilayered structure is an effective way to reduce the leakage current in BFO films [15]. In general, the buffer layer has different lattice constants. Thus the residual strain in ferroelectric thin films can be modulated, which results in changes of lattice distortion, dislocation formation, ferroelastic domain, etc. Consequently, the physical properties of ferroelectric thin films are influenced by the use of one or more buffer layers. For example, studies have shown that residual strain can greatly change the dielectric properties of ferroelectric $Pb_{0.92}La_{0.08}Zr_{0.52}Ti_{0.48}O_3$ (PZT) films [16], and that oxide buffer layers influence the electric and magnetic properties of BFO thin films [17,18]. In addition, the study of BFO films grown on various substrates with different lattice constants has also revealed that the planar stresses from lattice mismatch exert significant influence on the physical properties of the films [19].

2 Experimental details

In this work, $BaTiO_3$ (BTO) and $SrTiO_3$ (STO) were used as the buffers for BFO films. BTO and STO both have perovskite structures but with different lattice constants. In comparison to the rhombohedral BFO (a_{pc}=0.396 nm), tetragonal BTO has larger lattice parameters of a=0.399 nm and c=0.403 nm; by contrast, cubic STO has smaller lattice constants of a=0.391 nm. BFO/BTO and BFO/STO double-layer films were grown on $SrRuO_3$ (SRO)-covered STO substrates (100) by a pulsed laser deposition method. Lattice mismatch between the two layers can be compensated by residual strain. The present study shows that, as expected, the BFO layer in the BFO/BTO and the BFO/STO double-layer films suffers tensile strain and compressive strain, respectively, and thus their physical properties have been modified as well.

The ceramic targets used in the present study were synthesized by the conventional high-temperature solid-state reaction method. All of the layers in the films were deposited in sequence by using a XeCl 308 nm excimer laser with an energy density of around 1.5 J/cm^2 and a repetition of 2 Hz. During deposition, the oxygen pressure in the chamber was kept around 10 Pa and the substrate temperature determined by an infrared pyrometer was 590°C. After deposition, the samples were annealed for 10 min in the same environment. The BFO layer and BTO or STO buffer layers were equally controlled to be about 150 nm; the SRO bottom electrode was set to 50 nm. Pt dots with a diameter of 50 μm were grown on the BFO films as top electrodes.

3 Results and discussion

The crystal structures of the thin films were examined by an X-ray diffractometer (XRD) (Rigaku). The XRD patterns (not all shown here) indicate that the thin films were grown epitaxially, without any impurity. XRD patterns around the (002) peak of STO are shown in Figure 1. The $(002)_{pc}$ reflections for BFO, BTO, and SRO are identified; the dashed line shows the $(002)_{pc}$ peak location for BFO bulk. Compared to the BFO bulk, the BFO film on the BTO buffer has a $(002)_{pc}$ peak at a higher angle, whereas the BFO film on the STO buffer has a $(002)_{pc}$ peak at a lower angle. For a thin film layer, the shift of diffraction peaks is usually caused by strain resulting from a planar stress. It is known that a lower angle corresponds to a larger d-spacing in the out-of-plane direction induced by compress stress, whereas a higher angle indicates a smaller d-spacing induced by tensile stress. Because BFO has a smaller lattice than BTO and a larger lattice than STO, the BFO layer suffers tensile stress on a BTO buffer and compressive stress on an STO buffer. It is thus demonstrated that the BFO thin film on a BTO buffer undergoes tensile strain, whereas it undergoes compressive strain on a STO buffer.

In Figure 1, we see the XRD patterns around the (002) peak of STO. The $(002)_{pc}$ reflections for BFO, BTO, and SRO are identified. The dashed line shows the $(002)_{pc}$ peak location of the BFO bulk. Piezoresponse force microscopy (PFM) measurements were performed using an Asylum Research MFP-3D atomic force microscope with Si/Ir-coated tips at room temperature. Surface morphologies and phase images were taken simultaneously for one sample under PFM mode. The surface morphologies and out-of-plane phase images shown in Figure 2(a) and (c) are for the BFO/BTO sample; Figure 2(b) and (d) show results for the BFO/STO sample. Both of the films show island structures on their surfaces. The islands on the BFO/BTO sample are sphere-like whereas they are cuboid-like on the BFO/STO sample. The respective root-mean-square roughness of the two samples, which determined from the surface morphology images, is 2.9 and 3.3 nm. The BFO/BTO sample has a smoother surface. Out-

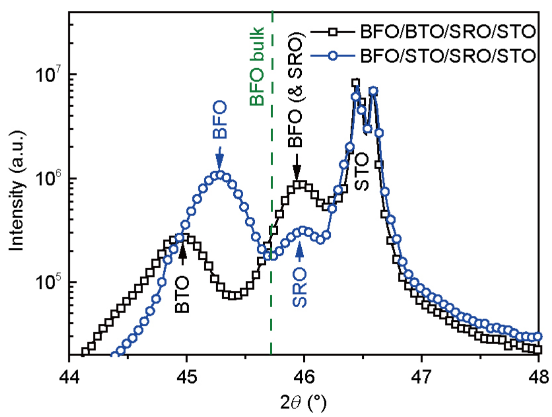

Figure 1 (Color online) XRD patterns around the (002) peak of STO. The $(002)_{pc}$ reflections for BFO, BTO, and SRO are identified. The dashed line shows the $(002)_{pc}$ peak location of the BFO bulk.

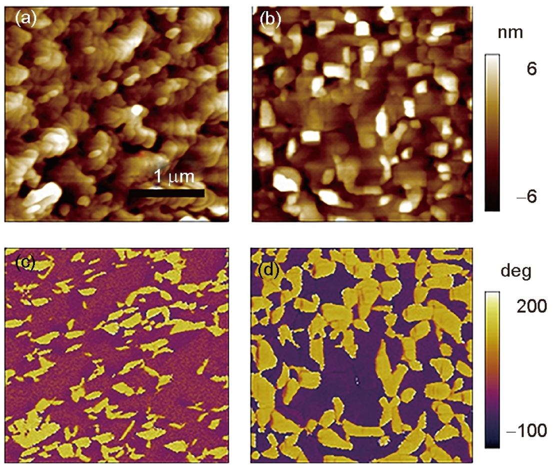

Figure 2 (Color online) Surface topographies and out-of-plane PFM phase images. (a) and (b) were obtained on the BFO/BTO sample; (c) and (d) were obtained on the BFO/STO sample.

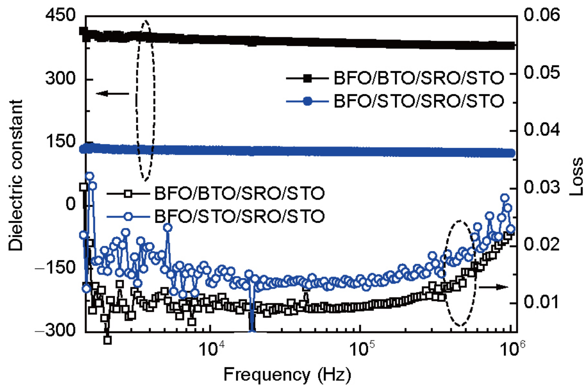

Figure 3 (Color online) Frequency dependence of capacitance and dielectric loss of Pt/BFO/BTO/SRO/STO and Pt/BFO/STO/SRO/STO heterostructure at room temperature.

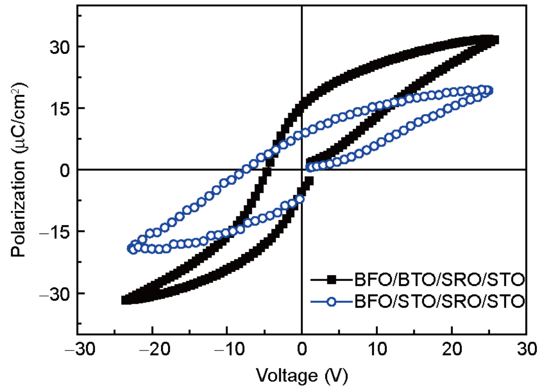

Figure 4 (Color online) *P-E* loops of Pt/BFO/BTO/SRO/STO and Pt/BFO/STO/SRO/STO heterostructure at room temperature. The test frequency is 10 kHz.

of plane domains are represented for BFO/BTO and BFO/STO in Figure 2(c) and (d). The purple regions indicate the ferroelectric domains have downward polarization, and the yellow regions indicate the upward domains. Thus, antiparallel domains in out-of-plane orientation are clearly seen in the PFM phase images for 180° contrast. The BFO/BTO sample has fewer upward domains with smaller size; by contrast, more than half of the domains in the BFO/STO sample are upward with larger size. Phase-field simulations have revealed that the domain structures and sizes of epitaxial BFO thin film are strongly dependent on the strain from substrate relating to elastic strain energy [20], electric boundary conditions [21], and other factors [22,23]. The compressive strain in the BFO thin film with the STO buffer would facilitate the formation of domains in out-of-plane orientation and consequently the formation of a larger domain. Our PFM results confirm and suggest that the domain structures in the BFO thin films are sensitive to the in-plane strain induced from either the BTO or STO buffer layer.

To investigate the strain effects of the buffer layers, we measured the electric properties of the BFO/BTO and BFO/STO samples in a capacitor structure with bottom electrode SRO and top electrode Pt dot. Figure 3 shows the frequency dependence of dielectric properties of the two samples. Neither sample is strongly sensitive to the testing frequency in the range of 1 kHz-1 MHz with capacitance and loss. However, the BFO/BTO sample shows larger permittivity (ε_r) and smaller dielectric loss than the BFO/STO sample.

We measured the polarization hysteresis (*P-E*) loops of the two samples using a ferroelectric test system (Radiant Technologies) at 100 kHz (Figure 4). The observed polarization hysteresis loops indicate that both of the samples show ferroelectricity, but neither is well saturated at the measured voltage range. Due to the unsaturation of the obtained ferroelectric loops, a comparison of their remnant polarizations would not make much sense here. The sample with BTO buffer has larger remnant polarization and smaller coercive voltage than the sample with STO buffer. However, both the samples with buffer show deterioration in dielectric and ferroelectric properties compared with the pure BFO thin films [24,25]. Therefore, the measured dielectric and ferroelectric properties of these two samples must be related to the properties of the buffer layer itself. The BTO buffer layer is ferroelectric and has larger permittivity than STO [26-28], which means that the BFO/STO film that composes a non-ferroelectric STO buffer layer has reduced permittivity or polarization. Moreover, the ferroelectric properties should be related to the domain configuration or stress state. Studies have shown that in-plane compressive strain leads to an increase in remnant and saturation polarizations in some ferroelectric materials, whereas tensile stress would decrease them [29]. These results may be attributed to the fact that compressive stress is beneficial to dipole alignment along the out-of-plane direction. According to the XRD and PFM results shown above, the in-plane tensile or compressive stress in the BFO film from the buffer layer exerts obvious influence on the domain configuration.

The current density-voltage (*J-V*) curves of the two samples measured by Aligent 2400 are shown in Figure 5. A density-voltage loop represents the current measured while the voltage is swept from negative to positive and back again to negative. The *J-V* loops obtained for both of the samples present asymmetrical *J-V* hysteresis, which indicates the rectifying characteristic and resistive switching behavior reported for BFO thin films without buffer [30]. The asymmetrical response would be caused by the different build-in potentials at the electrode interfaces. The potentials can be varied with ferroelectric polarization switching, which results in *J-V* hysteresis or resistive switching [31]. Compared with the *J-V* curves obtained on the unbuffered BFO films fabricated under similar conditions, the leakage currents of the two samples have been found to be largely reduced with the use of an insulating buffer layer [32]. Moreover, the BFO/BTO sample has smaller leakage than the BFO/STO, a result that can be ascribed in part to the difference of the electrical properties between BTO and STO (i.e, lower leakage current densities are found in BTO epitaxial film than in similar-thickness STO film [33,34]).

The large leakage currents in BFO thin films are in some sense due to the existence of Fe^{2+} and oxygen vacancies. Therefore, apart from the good insulating properties of the buffer layer itself, the reduction of the leakage current of the BFO with a BTO or STO buffer layer may be related to other, additional factors, such as the reduced oxygen vacancies in the BFO layer due to the introduction of Ti^{4+} [35] and the absorption of oxygen vacancies from BFO into the buffer layer [36].

Figure 6 shows in-plane and out-of plane magnetic hysteresis loops for both kinds of structures. As can be seen, either BFO/BTO/SRO/STO or BFO/STO/SRO/STO structure exhibits ferromagnetic hysteresis loops and their saturations. We also calculated the diamagnetic background from STO substrate and subtracted it from the new data. In both conditions, it is obvious that higher in-plane than out-of plane magnetization was obtained for buffered BFO films. Moreover, BFO film with a BTO buffer layer has higher magnetization according to both types of measurement. For BFO/BTO films, the respective in-plane saturated and remnant magnetizations were 10.6 and 5.5 emu/cm^3, whereas for the out-of plane magnetization they are 7.3 and 3.1 emu/cm^3. As previously reported, our results are analogous to other studies about the magnetic properties of single-layer BFO film [37]. Large strain is considered an effective way to adjust the phase and magnetic property of BFO film, both in experiments and theoretical calculations [14].

In our work, we have found that tensile strain created by a BTO buffer layer enhances the magnetic property of BFO film. However, as reported by Dupé et al. [38], when driven by the coupling between magnetism and oxygen octahedral tilting, the magnetization decreases under tensile strain. It has also been observed, however, that the magnetic value of BFO film compressed by a STO buffer layer does not increase—a result in agreement with other reports of the BFO/PZT structure [39-41]. In addition, the Shelke group stated that either tensile or compressive strain makes small contributions to the magnetic moment of BFO film [42]. In general, the intrinsic characteristics of two buffer materials also influence the final magnetic properties. It is the combination of coefficient consequence, strain, and the buffer layers' own properties that contribute to magnetization [43,44]. The precise underlying mechanism of this combined effect has yet to be determined.

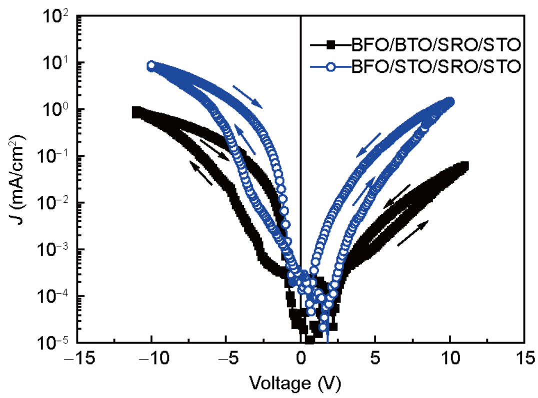

Figure 5 (Color online) *J-V* curves of Pt/BFO/BTO/SRO/STO and Pt/BFO/STO/SRO/STO heterostructure at room temperature.

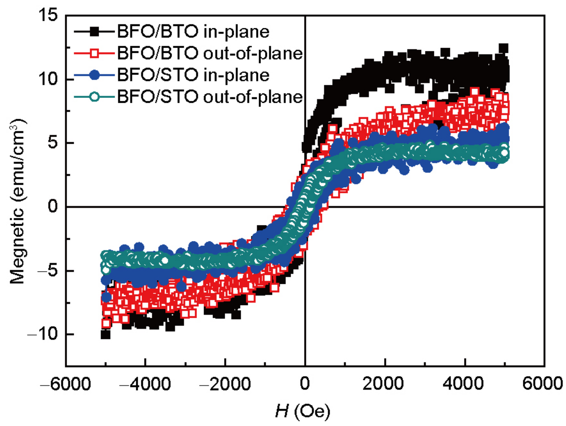

Figure 6 (Color online) *M-H* curves of Pt/BFO/BTO/SRO/STO and Pt/BFO/STO/SRO/STO heterostructure at room temperature.

4 Conclusions

In summary, we grew epitaxial BFO thin films with BTO or STO buffer layers. It is demonstrated that the in-plane strain in BFO thin films can be engineered to be tensile strain or compressive strain by the use of either a BTO or STO buffer layer, due to differences in their lattice parameters. The ferroelectric domain structures as well as the electrical properties of the BFO/BTO and BFO/STO show obvious dependence on the buffer layer. Compared to the BFO thin films without buffer, the leakage currents densities of the BFO/BTO and BFO/STO samples were reduced; the ferroelectric properties of the samples, however, were deteriorated. Apart from the modulated strain, the intrinsic properties of the buffer layer play an important role in the electrical and magnetic properties of the samples. The present study indicates that by using an appropriate buffer layer, the physical properties of BFO thin film can be artificially engineered and optimized for special application.

This work was supported by the National Key Basic Research Program of China (Grant Nos. 2014CB921002, and 2013CBA01703), the National Natural Science Foundation of China (Grant Nos. 11174355, 11674385, and 11574365), and the Strategic Priority Research Program (B) of the Chinese Academy of Sciences (Grant No. XDB07030200).

1 C. Ederer, and N. A. Spaldin, Nat. Mater. **3**, 849 (2004).
2 C. Blaauw, and F. van der Woude, J. Phys. C-Solid State Phys. **6**, 1422 (1973).
3 G. A. Smolenskiĭ, and I. E. Chupis, Sov. Phys. Usp. **25**, 475 (1982).
4 J. B. Neaton, C. Ederer, U. V. Waghmare, N. A. Spaldin, and K. M. Rabe, Phys. Rev. B **71**, 014113 (2005).
5 R. Seshadri, and N. A. Hill, Chem. Mater. **13**, 2892 (2001).
6 R. Y. Zheng, C. H. Sim, J. Wang, and S. Ramakrishna, J. Am. Ceramic Soc. **91**, 3240 (2008).
7 T. T. Shang, X. Y. Liu, and L. Gu, Sci. China-Phys. Mech. Astron. **59**, 697001 (2016).
8 J. N. Ding, M. J. Chen, J. H. Qiu, and N. Y. Yuan, Sci. China-Phys. Mech. Astron. **58**, 037701 (2015).
9 T. B. Wu, C. M. Wu, and M. L. Chen, Appl. Phys. Lett. **69**, 2659 (1996).
10 G. Gerra, A. K. Tagantsev, N. Setter, and K. Parlinski, Phys. Rev. Lett. **96**, 107603 (2006).
11 B. Chen, H. Yang, L. Zhao, J. Miao, B. Xu, X. G. Qiu, B. R. Zhao, X. Y. Qi, and X. F. Duan, Appl. Phys. Lett. **84**, 583 (2004).
12 C. S. Hwang, J. Appl. Phys. **92**, 432 (2002).
13 X. J. Zheng, Y. C. Zhou, and J. Y. Li, Acta Mater. **51**, 3985 (2003).
14 J. Wang, J. B. Neaton, H. Zheng, V. Nagarajan, S. B. Ogale, B. Liu, D. Viehland, V. Vaithyanathan, D. G. Schlom, U. V. Waghmare, N. A. Spaldin, K. M. Rabe, M. Wuttig, and R. Ramesh, Science **299**, 1719 (2003).
15 H. R. Liu, Y. X. Sun, and X. Z. Wang, J. Phys. D-Appl. Phys. **41**, 095302 (2008).
16 B. Ma, S. Liu, S. Tong, M. Narayanan, and U. (Balu) Balachandran, J. Appl. Phys. **112**, 114117 (2012).
17 R. Y. Zheng, J. Wang, and S. Ramakrishna, J. Appl. Phys. **104**, 034106 (2008).
18 J. Wu, and J. Wang, J. Appl. Phys. **105**, 124107 (2009).
19 J. X. Zhang, Y. L. Li, S. Choudhury, L. Q. Chen, Y. H. Chu, F. Zavaliche, M. P. Cruz, R. Ramesh, and Q. X. Jia, J. Appl. Phys. **103**, 094111 (2008).
20 Y. H. Chu, T. Zhao, M. P. Cruz, Q. Zhan, P. L. Yang, L. W. Martin, M. Huijben, C. H. Yang, F. Zavaliche, H. Zheng, and R. Ramesh, Appl. Phys. Lett. **90**, 252906 (2007).
21 Y. L. Li, S. Y. Hu, Z. K. Liu, and L. Q. Chen, Appl. Phys. Lett. **78**, 3878 (2001).
22 Z. Luo, Z. Chen, Y. Yang, H. J. Liu, C. Huang, H. Huang, H. Wang, M. M. Yang, C. Hu, G. Pan, W. Wen, X. Li, Q. He, T. Sritharan, Y. H. Chu, L. Chen, and C. Gao, Phys. Rev. B **88**, 064103 (2013).
23 G. Catalan, J. Seidel, R. Ramesh, and J. F. Scott, Rev. Mod. Phys. **84**, 119 (2012).
24 H. Uetake, S. Yabukami, T. Chiba, T. Ozawa, H. Suzuki, N. Kobayashi, and K. I. Arai, J. Magn. Soc. Jpn. **38**, 83 (2014).
25 L. Pálová, P. Chandra, and K. M. Rabe, Phys. Rev. B **76**, 014112 (2007), arXiv: 0704.2752.
26 Z. Yao, C. Wang, Y. Li, H. K. Kim, and N. Y. Kim, Nanoscale Res. Lett. **9**, 435 (2014).
27 N. M. Murari, R. Thomas, S. P. Pavunny, J. R. Calzada, and R. S. Katiyar, Appl. Phys. Lett. **94**, 142907 (2009).
28 J. Wu, and J. Wang, J. Appl. Phys. **108**, 034102 (2010).
29 J. W. Lee, G. T. Park, C. S. Park, and H. E. Kim, Appl. Phys. Lett. **88**, 072908 (2006).
30 C. Ge, K. J. Jin, C. Wang, H. B. Lu, C. Wang, and G. Z. Yang, Appl. Phys. Lett. **99**, 063509 (2011).
31 X. Qi, J. Dho, R. Tomov, M. G. Blamire, and J. L. MacManus-Driscoll, Appl. Phys. Lett. **86**, 062903 (2005).
32 H. Yang, M. Jain, N. A. Suvorova, H. Zhou, H. M. Luo, D. M. Feldmann, P. C. Dowden, R. F. DePaula, S. R. Foltyn, and Q. X. Jia, Appl. Phys. Lett. **91**, 072911 (2007).
33 S. H. Paek, E. S. Lee, S. H. Kim, and J. Y. Seong, J. Mater. Sci. **33**, 1239 (1998).
34 M. Iwabuchi, and T. Kobayashi, J. Appl. Phys. **75**, 5295 (1994).
35 A. Gruverman, D. Wu, H. Lu, Y. Wang, H. W. Jang, C. M. Folkman, M. Y. Zhuravlev, D. Felker, M. Rzchowski, C. B. Eom, and E. Y. Tsymbal, Nano Lett. **9**, 3539 (2009), arXiv: 0906.1521.
36 G. L. Yuan, L. W. Martin, R. Ramesh, and A. Uedono, Appl. Phys. Lett. **95**, 012904 (2009).
37 J. Chang, H. M. Jang, and S. K. Kim, J. Magn. **11**, 108 (2006).
38 B. Dupé, S. Prosandeev, G. Geneste, B. Dkhil, and L. Bellaiche, Phys. Rev. Lett. **106**, 237601 (2011).
39 S. H. Lee, S. P. Nam, S. G. Bae, and Y. H. Lee, J. Ceram. Process Res. **13**, 188 (2012).
40 C. J. Cheng, C. Lu, Z. Chen, L. You, L. Chen, J. Wang, and T. Wu, Appl. Phys. Lett. **98**, 242502 (2011).
41 A. Agbelele, D. Sando, I. C. Infante, C. Carrétéro, S. Jouen, J. M. Le Breton, A. Barthélémy, B. Dkhil, M. Bibes, and J. Juraszek, Appl. Phys. Lett. **109**, 042902 (2016).
42 V. Shelke, D. Mazumdar, G. Srinivasan, and A. Gupta, J. Appl. Phys. **109**, 07D914 (2011).
43 P. Yang, K. M. Kim, Y. G. Joh, D. H. Kim, J. Y. Lee, J. Zhu, and H. Y. Lee, J. Appl. Phys. **105**, 061618 (2009).
44 V. Kumar, A. Gaur, R. J. Chaudhury, and D. Kumar, Superl. Microstruct. **98**, 54 (2016).